Climatic Consequences of a Large-Scale Desertification in Northeast Brazil: A GCM Simulation Study

MARCOS DAISUKE OYAMA* AND CARLOS AFONSO NOBRE

Centro de Previsão de Tempo e Estudos Climáticos, Instituto Nacional de Pesquisas Espaciais, Cachoeira Paulista, São Paulo, Brazil

(Manuscript received 1 October 2003, and in final form 13 February 2004)

ABSTRACT

The climatic impacts of a large-scale desertification in northeast Brazil (NEB) are assessed by using the Center for Weather Forecasting and Climate Studies–Center for Ocean–Land–Atmosphere Studies (CPTEC–COLA) AGCM. Two numerical runs are performed. In the control run, NEB is covered by its natural vegetation (most of NEB is covered by a xeromorphic vegetation known as *caatinga*); in the desertification run, NEB vegetation is changed to desert (bare soil). Each run consists of five 1-yr numerical integrations. The results for NEB wet season (March–May) are analyzed. Desertification results in hydrological cycle weakening: precipitation, evapotranspiration, moisture convergence, and runoff decrease. Surface net radiation decreases and this reduction is almost evenly divided between sensible and latent heat flux. Atmospheric diabatic heating decreases and subsidence anomalies confined at lower atmospheric levels are found. The climatic impacts result from the cooperative action of feedback processes related to albedo increase, plant transpiration suppression, and roughness length decrease. On a larger scale, desertification leads to precipitation increase in the oceanic belt close to the northernmost part of NEB (NNEB). In the NEB–NNEB dipole, the anomalies of vertical motion and atmospheric circulation are confined to lower atmospheric levels, that is, 850–700 hPa. At these levels, circulation anomalies resemble the linear baroclinic response of a shallow atmospheric layer (850–700 hPa) to a tropical heat sink placed over NEB at the middle-layer level. Therefore, NEB climate does show sensitivity to a vegetation change to desert. The present work shows the possibility of significant and pronounced climate impacts, on both regional and large scales, if the environmental degradation in NEB continues unchecked.

1. Introduction

Wet climate and tropical forests are generally found within the equatorial zone (roughly between 10°S and 10°N). However, in northeast Brazil (NEB; 1°–18°S, 47°–35°W), there is a large semiarid area covered by a xeromorphic vegetation known as *caatinga*. These climate and vegetation features are atypical for a continental equatorial region (Nobre and Molion 1988). In the semiarid area of NEB, annual precipitation is on average less than 800 mm and is subjected to large interannual variability (Hastenrath and Heller 1977). The rainy season extends from February to May, when the intertropical convergence zone (ITCZ) reaches its southernmost position.

Currently, more than 10% of the semiarid area of NEB has already undergone a very high degree of environmental degradation (MMA 2000; Fig. 1). The driest areas of NEB, that is, those with average annual precipitation less than 500 mm, are the most susceptible to desertification, and about 65% of its area is seriously affected by environmental degradation processes (Sá et al. 1994). As in other parts of the world, improper land use is the main factor for environmental degradation in NEB (Ferreira et al. 1994). Recently, the Brazilian government has approved an official conservation policy for NEB (named National Desertification Combat Plan) to regenerate degraded areas and to avoid further environmental degradation (CONAMA 1997).

There is observational evidence that the increasing environmental degradation in NEB has not been able as yet to affect the rainfall regime (Silva et al. 1998). However, if actual conservation initiatives were not able to slow down or reverse the process of environmental degradation, the decrease in soil fertility, primary productivity, and water resources availability could lead to a large-scale anthropogenic desertification in NEB. In this scenario, would precipitation—or, in a more general

* Current affiliation: Centro Técnico Aeroespacial, Instituto de Aeronáutica e Espaço, São José dos Campos, São Paulo, Brazil.

Corresponding author address: Dr. Marcos Daisuke Oyama, Centro Técnico Aeroespacial, Instituto de Aeronáutica e Espaço, Divisão de Ciências Atmosféricas, Pça Marechal Eduardo Gomes, 50, Vila das Acácias, 12228-904, São José dos Campos, SP, Brazil.
E-mail: oyama@iae.cta.br

© 2004 American Meteorological Society

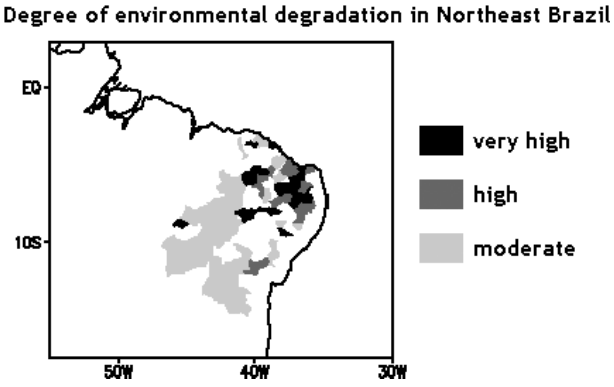

FIG. 1. Environmental degradation degree in NEB according to the Brazilian Ministry of the Environment. Adapted from MMA (2000, p. 9).

sense, climate—be affected? In the present work, the climatic impacts of a large-scale desertification in NEB are assessed with the use of an atmospheric general circulation model (AGCM).

2. Established background of the study

It is known that vegetation change affects microclimate, that is, the radiation, energy, and water budgets at the surface. If the vegetation change takes place over large areas, then the impacts could not be restricted to the lower atmospheric levels (surface and boundary layer), but could change both regional and large-scale atmospheric circulation. There are two opposing viewpoints regarding the atmospheric circulation response to evapotranspiration anomalies due to vegetation change (Zeng et al. 1996, p. 859). The first (second) holds that evapotranspiration and atmospheric moisture convergence anomalies would have opposite signs (the same sign); climate sensitivity to land cover changes would be low (high). The second viewpoint is supported by results of modeling studies on the effects of large-scale deforestation in Amazonia (e.g., Nobre et al. 1991). According to the majority of predictions (McGuffie and Henderson-Sellers 2001, p. 1100), precipitation, evapotranspiration, and moisture convergence would decrease in Amazonia.

Several mechanisms have been proposed to explain how land cover changes could affect climate (Sellers 1992, 457–460; Dickinson 1992, 690–696; Sud et al. 1993; Dirmeyer and Shukla 1996). For instance, consider the effects of desertification on precipitation. Albedo increase, other things being equal, results in net radiation decrease at the top of the atmosphere (TOA), thus inducing subsidence that inhibits precipitation (albedo mechanism; Charney 1975; Charney et al. 1977). Plant transpiration suppression results in a drier boundary layer (particularly over the dry and transition seasons), thus decreasing water vapor availability to weather precipitating systems (evapotranspiration mechanism; Charney et al. 1977; Shukla and Mintz 1982). Roughness length reduction results, on the one hand, in less mass convergence around surface low pressure centers, thus decreasing the upward moisture transport that feeds into convective precipitating clouds (roughness mechanism; Sud et al. 1988); on the other hand, in less turbulent fluxes, thus decreasing precipitation by processes similar to albedo and evapotranspiration mechanisms. The three mechanisms operate positive feedback loops, since precipitation decrease favors more desertification.

To investigate climate sensitivity to land cover changes, AGCMs have been used. For Sahel, the semiarid region in the southern Sahara, several AGCM studies (e.g., Charney et al. 1977; Sud and Fennessy 1982, 1984; Xue and Shukla 1993; Dirmeyer and Shukla 1996) reveal that land cover degradation would result in precipitation decrease. This is an almost consensual conclusion obtained from several different AGCMs.

For NEB, only three AGCM studies evaluate climate sensitivity to land cover change. Sud and Fennessy (1982, 1984; hereafter SF82 and SF84, respectively) performed 45-day simulations using simple land surface parameterizations within a low-resolution AGCM. They found that desertification in NEB (change to bare soil albedo in SF82, and to zero evaporation in SF84) would decrease precipitation by about 0.4 mm day^{-1}. Dirmeyer and Shukla (1996; hereafter DS96) performed 10-yr simulations using a sophisticated biophysical model, the Simplified Simple Biosphere model (SSiB; Xue et al. 1991), within a low-resolution AGCM. They found that a change to semidesert vegetation in NEB would not affect the regional annual precipitation.

The DS96 conclusion that NEB climate would not be sensitive to land cover degradation deserves further testing, since NEB climate could be sensitive to a more pronounced environmental degradation, for example, replacement of NEB vegetation by bare soil, as suggested by SF82 and SF84 results. Therefore, in the present work, the climatic impacts are assessed by changing the NEB vegetation to desert (bare soil). Furthermore, 1) as only one region (NEB) is focused on, a detailed account of the land and atmosphere processes responsible for the climatic impacts is given (unlike SF82, SF84, and DS96, which studied several regions); 2) SSiB is used as land surface scheme (similarly to DS96); 3) a medium-resolution AGCM is used (unlike SF82, SF84, and DS96, which used low-resolution AGCMs). This higher resolution allows for better resolving the ITCZ, which is the main control of NEB climate.

3. Model

The Center for Weather Forecasting and Climate Studies–Center for Ocean–Land–Atmosphere Studies AGCM, hereafter referred to as CPTEC–COLA AGCM, is used for the numerical simulations. Its main features are described in Cavalcanti et al. (2002) and Kinter et

TABLE 1. Annual average of albedo (α), roughness length (z_0), and vegetation cover fraction (υ) for tropical forest, savanna, caatinga, semidesert vegetation, and desert (bare soil). Vegetation classification follows Dorman and Sellers (1989).

Biome	Name	α (%)	z_0 (m)	υ (%)
1	Tropical forest	13	2.65	98
6	Savanna	20	0.85	30
8	Caatinga	23	0.24	10
9	Semidesert	31	0.07	10
11	Desert	35	0.01	0

al. (1997). Model resolution is T62L28, that is, 28 levels and horizontal resolution of about 2°.

The land surface scheme within the CPTEC–COLA AGCM is the SSiB. It is a big leaf model that calculates the radiation, energy, and water budgets at the surface. Biophysical models like SSiB represent the land surface processes in a detailed manner and provide a more realistic surface energy partition, avoiding numerical instabilities during the integration of the surface water budget equations (Sato et al. 1989).

For each land grid point, a vegetation type (biome) is prescribed. The vegetation classification follows Dorman and Sellers (1989). A set of physical, morphological, and physiological parameters is assigned to each biome. For illustration purposes, the annual average of albedo, vegetation cover fraction, and roughness length for tropical forest, savanna, caatinga, semidesert vegetation, and desert (bare soil) are shown in Table 1. While vegetation cover fraction and roughness length are prescribed parameters, albedo (α) is calculated as $\alpha = a_1 + b_1\mu + c_1\mu^2$, where a_1, b_1, and c_1 are coefficients calibrated for each biome, and μ is the cosine of the zenital angle. The parameters may vary seasonally.

Recently, the CPTEC–COLA AGCM was validated for present-day climatic simulations (Cavalcanti et al. 2002). The model is able to reproduce the main atmospheric large-scale features (e.g., global energy balance, zonally average circulation, convergence zones, etc.). On the regional level, however, systematic errors are found. For instance, precipitation is underestimated in parts of Amazonia and overestimated in NEB. This systematic error is also found in numerous other AGCMs (e.g., Lau et al. 1996). Despite the presence of systematic errors, the CPTEC–COLA AGCM is able to reproduce the observed interannual variability of both Amazonia and NEB (Marengo et al. 2003).

In the present work, the assessment of climate impacts is based on anomaly values (i.e., difference between simulation and control runs; the numerical runs are described in section 4). Due to the existence of systematic errors, it is necessary to assign uncertainties to the calculated anomalies; the lower the systematic error, the lower the uncertainty (Sud et al. 1996, p. 3226). The degree of uncertainty of the present work assessments is the same as DS96. The AGCM used in DS96—COLA AGCM—overestimates the precipitation in NEB and the magnitude of the systematic error is similar to CPTEC–COLA AGCM. This is expected since CPTEC–COLA AGCM builds upon COLA AGCM (Cavalcanti et al. 2002). In DS96, as in the present work, NEB is one of the studied regions.

4. Simulations

Two runs are performed. In the control run, NEB is covered by its natural vegetation (most of NEB is covered by *caatinga*; Fig. 2a). In the simulation or desertification run, NEB vegetation is changed to desert (bare soil; Fig. 2b). Each run consists of five 1-yr numerical integrations, called members (i.e., each member is related to a 1-yr run). Table 2 shows the atmospheric initial condition and the sea surface temperature (SST) boundary condition for each member. Three of the five members (members 1, 2, and 3) refer to different atmospheric initial conditions, 15, 16, and 17 November 1998, for the same SST boundary condition—climatological SST. The remaining two members (members 4 and 5) refer to different boundary conditions—observed SST in 1983 (dry year in NEB according to simulations per-

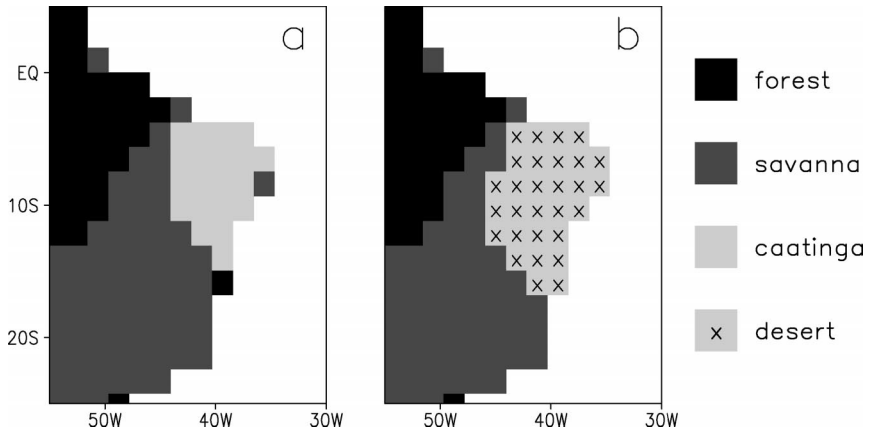

FIG. 2. Vegetation maps for the (a) control and (b) desertification runs.

TABLE 2. Initial and boundary conditions for each ensemble member.

Member No.	Atmospheric initial condition	SST
1	15 Nov 1998	Climatology
2	16 Nov 1998	Climatology
3	17 Nov 1998	Climatology
4	15 Nov 1998	1983
5	15 Nov 1998	1985

TABLE 3. Sign test statistical significance levels for five realizations. Here, N_+ is the number of positive sign anomalies.

N_+	Significance level (%)	Terminology
5 or 0	94	High significance
4 or 1	68	Low significance
3 or 2	38	No significance

formed by Cavalcanti et al. 2002) and 1985 (wet year)—for the same initial condition of 15 November 1998. The number of members and the strategy of including observed (SST) conditions associated with wet and dry years follow Xue and Shukla (1993).

The numerical integrations start around mid-November and extend until the last day of the subsequent year. The first 45 days of each integration are neglected due to soil moisture spinup. In both runs, soil moisture is initialized using the CPTEC–COLA AGCM soil moisture equilibrium values (model climatology from Cavalcanti et al. 2002) for November. Oyama et al. (2000) showed that this initialization (instead of using observed soil moisture) leads to a soil moisture spinup time of less than 1 month for the control run; thus, the neglected 45 days are enough for soil moisture adjustment.

For each run, five-member ensemble averages are taken to filter out the AGCM intermember variability. The statistical significance of the anomalies is evaluated using the Student's *t* test and/or the sign test. It is expected that members 4 and 5 (Table 2) increase the ensemble anomaly variance and thus decrease the *t* statistic. Therefore, very high anomaly values are needed to attain statistical significance using the Student's *t* test. To single out the most robust changes, the Student's *t* test is used for evaluating the regional impacts of NEB desertification (section 5). Outside NEB, to disregard the effect of variance increase introduced by members 4 and 5 on statistical significance, the sign test is added. It may be regarded as a less restrictive significance test (thus enlarging the regions with significant anomalies), and is mainly used for evaluating the remote changes due to NEB desertification (section 6). In the sign test, for each member, the anomaly sign is scored. In Table 3, the statistical significance as a function of the number of positive anomalies is shown, as well as the terminology hereafter used. We shall consider that there is statistical significance by the sign test if the number of positive anomalies is ≥ 4 or ≤ 1.

5. Regional changes

On annual average, desertification leads to a pronounced precipitation decrease in western NEB (Fig. 3a). The anomalies are statistically significant (99% confidence level in Student's *t* test; see Fig. 4a) and show magnitudes greater than 1.5 mm day^{-1}. These anomalies result from the pronounced and statistically significant (99% confidence level in Student's *t* test) precipitation decrease of about 3 mm day^{-1} in the wet season (Figs. 3b and 4b). The inclusion of members forced by nonclimatological SST (members 4 and 5; see

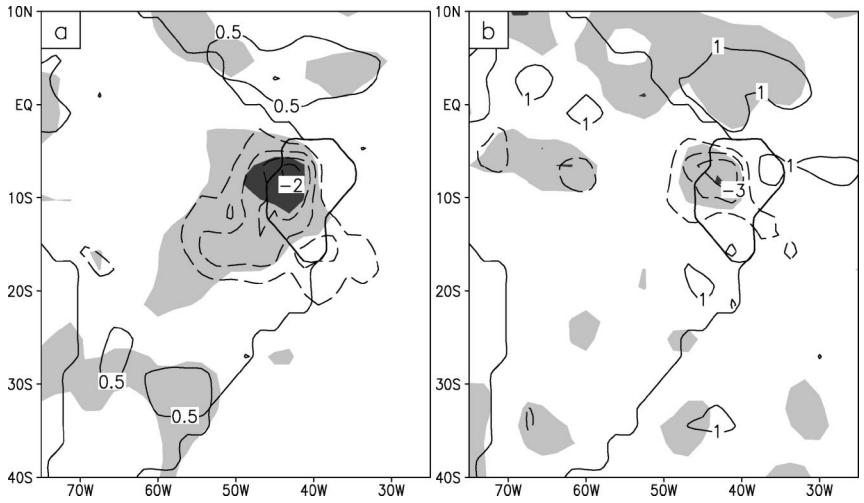

FIG. 3. (a) Annual and (b) wet season (Mar–May) precipitation anomalies. Contour interval is 0.5 in (a) and 1 mm day^{-1} in (b). Solid (dashed) lines refer to positive (negative) values; zero line is omitted. Dark and light shading refer to high and low statistical significance anomalies, respectively, for the sign test. NEB is enclosed by a thick contour line.

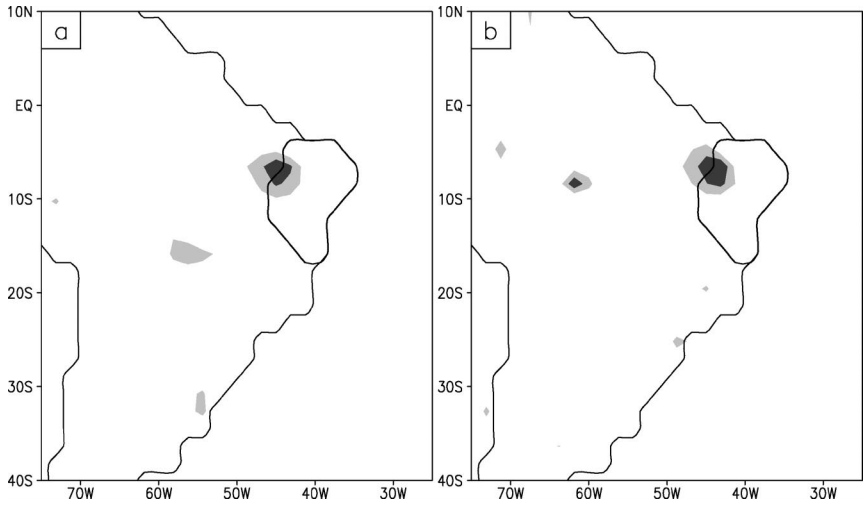

FIG. 4. (a) Annual and (b) wet season (Mar–May) precipitation anomaly statistical significance using Student's *t* test. Dark and light shading refer to 99% and 95% confidence levels, respectively. NEB is enclosed by a thick contour line.

Table 2) does not change the precipitation anomalies pattern, but increases the anomalies variance in NEB and other regions (not shown). Therefore, NEB climate, both annually and seasonally, does show climate sensitivity to a land cover change to desert (bare soil). It ratifies and expands previous assessments based on 45-day integrations using simple land surface parameterizations within a low-resolution AGCM (SF82, SF84).

The different sensitivities obtained by the present work and DS96 may be explained as follows. In DS96, the land cover in NEB is replaced by semidesert vegetation; in the present work, by desert (bare soil). Therefore, the results of the present work and DS96 may be regarded as complementary; taking them together, we can conclude that, for ''small'' changes in NEB vegetation—for example, caatinga to semidesert vegetation—the current climate state would not change; but, for ''large'' changes—for example, caatinga to desert (bare soil)—climate would become drier (i.e., with less precipitation). This nonlinear biome–climate relation, however, may be different if vegetation change in other regions is taken into account. Oyama and Nobre (2003) showed that even a degradation of lesser degree in NEB—conversion to semidesert vegetation only in the driest region of NEB—could lead to significant precipitation decrease in the driest region of NEB if vegetation change from forest to savanna also takes place in eastern Amazonia.

In what follows, the regional climate changes in NEB (i.e., areal average over NEB) are shown. The anomalies for NEB wet season (March to May) are analyzed, since the most pronounced changes in precipitation occur in the wet season (not shown). Table 4 presents the desertification effects on many variables.

The hydrological cycle weakens: precipitation, evapotranspiration, atmospheric moisture convergence, and runoff decrease. The evapotranspiration decrease is due to plant transpiration suppression. Evapotranspiration and moisture convergence anomalies act in the same direction (i.e., have the same sign); hence, atmospheric circulation does not act as a restoring mechanism. At the surface, the hydrological cycle weakening is related to an almost uniform soil moisture reduction in all layers. Runoff decreases due to a decrease in both soil moisture and precipitation. Gibbs effect due to the Andes mountain range results in a closing error for the atmospheric water budget (not shown). This error, however, is not statistically significant and would disappear if more members were included in the ensemble.

Desertification results in an albedo and surface air temperature increase, and cloudiness decrease. Cloudiness decrease is probably related to precipitation reduction. Surface net radiation decreases since its shortwave and longwave components both decrease. In the shortwave radiation budget, incident (downward) radiation increase due to cloudiness decrease compensates only part of reflected (upward) radiation increase due to albedo increase. In the longwave radiation budget, upward radiation increases due to surface air temperature increase, while downward radiation decreases due to cloudiness decrease.

Surface net radiation reduction is almost evenly divided between sensible and latent heat flux. The reduction in both turbulent fluxes result in drier and cooler reference level (Z_R, lowest AGCM level, about 970 hPa for NEB), but the changes in temperature and humidity at Z_R are small (not shown). The turbulent fluxes reduction should be related to increase in surface resistances (particularly aerodynamic resistance), not to changes in temperature and/or moisture vertical gradients (since temperature increase at the surface and decrease at Z_R favor increase in sensible heat flux).

TABLE 4. Wet season (Mar–May) regional (that is, area average over NEB) impacts of desertification. Here, SW_{up} (LW), SW_{down} (LW), and ΔSW (LW) refer to upward, downward, and net shortwave (longwave) radiation, respectively; sfc and TOA refer to surface and top of the atmosphere, respectively; Z_R refers to the reference level (lowest AGCM level); and W refers to the soil moisture degree of saturation. Anomaly values are the difference between simulation and control values.

Variable	Unit	Anomaly	Variable	Unit	Anomaly
Precipitation	mm day^{-1}	−0.85	$SW_{down,sfc}$	W m^{-2}	+20.1
Evapotranspiration	mm day^{-1}	−0.30	$SW_{up,sfc}$	W m^{-2}	+28.1
Moisture convergence	mm day^{-1}	−0.81	ΔSW_{sfc}	W m^{-2}	−8.0
Runoff	mm day^{-1}	−0.32	$LW_{down,sfc}$	W m^{-2}	−2.7
W	%	−10	$LW_{up,sfc}$	W m^{-2}	+6.1
Albedo	%	+10	ΔLW_{sfc}	W m^{-2}	−8.8
Surface air temperature	K	+1.2	Surface net radiation	W m^{-2}	−16.8
Total cloudiness	%	−6	$SW_{up,TOA}$	W m^{-2}	+8.5
Sensible heat flux	W m^{-2}	−8.4	$LW_{up,TOA}$	W m^{-2}	+8.3
Latent heat flux	W m^{-2}	−8.6	Net radiation at TOA	W m^{-2}	−16.8
Surface pressure	hPa	+0.2	Atmospheric net radiation	W m^{-2}	0.0
Zonal wind at Z_R	m s^{-1}	−1.0	Diabatic heating	W m^{-2}	−32.5
Meridional wind at Z_R	m s^{-1}	0.0	Adiabatic warming	W m^{-2}	+35.7

Regionally, circulation changes at Z_R are shown in Table 4. Desertification enhances the easterly flow at Z_R over NEB (Figs. 5a,b). The wind anomalies bring forth subsidence anomalies in NEB and upward motion anomalies in the westernmost part of NEB. The vertical velocity anomalies have small magnitude (ranging from 10^{-7} to 10^{-8} cb s^{-1}) and are mainly related to changes in zonal wind (Fig. 5c). The easterly flow enhancement is confined to NEB.

Desertification results in a small Bowen ratio decrease (from 0.36 to 0.30). In general, the drier the climate, the greater the Bowen ratio (e.g., Stull 1988, p. 274). Therefore, Bowen ratio reduction is contrary to the expected. It results from the sufficiently pronounced sensible heat flux reduction that overcomes the latent heat flux decrease effects on Bowen ratio. The sensible heat flux decrease should be related to a marked increase in aerodynamic resistance due to decrease in roughness length. Under neutral conditions, assuming a log wind profile, the aerodynamic resistance increase would be of about 6 times. This increase is related to a decrease in surface-layer turbulent momentum mixing; friction velocity would decrease by a factor of 2.

There is a negligible increase in surface pressure. As mentioned earlier, surface air temperature increases. Therefore, surface pressure increase, albeit negligible, demonstrates that the negative feedback mechanism proposed by SF84—in which evapotranspiration reduction results in higher surface temperature, lower surface pressure, and enhancement of low-level convergence—is not operating.

Net radiation reduction at the surface is transferred to TOA; thus, atmospheric radiative cooling is not affected by desertification. Diabatic heating decreases mainly due to latent heat release (related to precipitation) reduction. To keep atmospheric thermal balance, adiabatic warming increases. Since changes in static stability and temperature profile are negligible (not shown), adiabatic warming anomalies are due to changes in vertical velocity profile.

Subsidence anomalies take place throughout the atmospheric column (Table 5), reaching maximum magnitude between 850 and 700 hPa. Therefore, atmospheric divergence anomalies are found between 850 hPa and Z_R, and convergence anomalies, between 700 and 500 hPa. Above 500 hPa, atmospheric divergence or convergence anomalies are negligible.

In the Z_R–850-hPa layer, moisture divergence anomalies are found (Table 6), since there are atmospheric divergence anomalies in this layer. In the 850–700-hPa layer, small moisture divergence differences are found; it may be regarded as a transition layer where moisture convergence anomalies change sign. In the 700–500-hPa layer, moisture convergence anomalies are found, since there are atmospheric convergence anomalies in this layer. Thus, there is moisture divergence anomaly between Z_R and 700 hPa, and moisture convergence anomaly between 700 and 500 hPa. Above 500 mb, moisture convergence or divergence anomalies are negligible. The pronounced moisture divergence anomaly in the Z_R–850-hPa layer is responsible for the vertically integrated moisture convergence reduction.

NEB desertification leads to significant regional climatic changes. The impacts result from vegetation–atmosphere feedback mechanisms. First, the evapotranspiration mechanism could be operating, since precipitation and evapotranspiration both decrease. The evapotranspiration reduction, however, does not have enough strength to bring about the negative feedback mechanism proposed by SF84, since desertification does not lead to surface thermal low anomalies. Second, moisture convergence decrease could be related to albedo mechanism. Net radiation at TOA decreases in part due to albedo increase; to keep atmospheric thermal balance, subsidence anomalies emerge and result in atmospheric divergence anomalies at lower atmospheric levels, thus

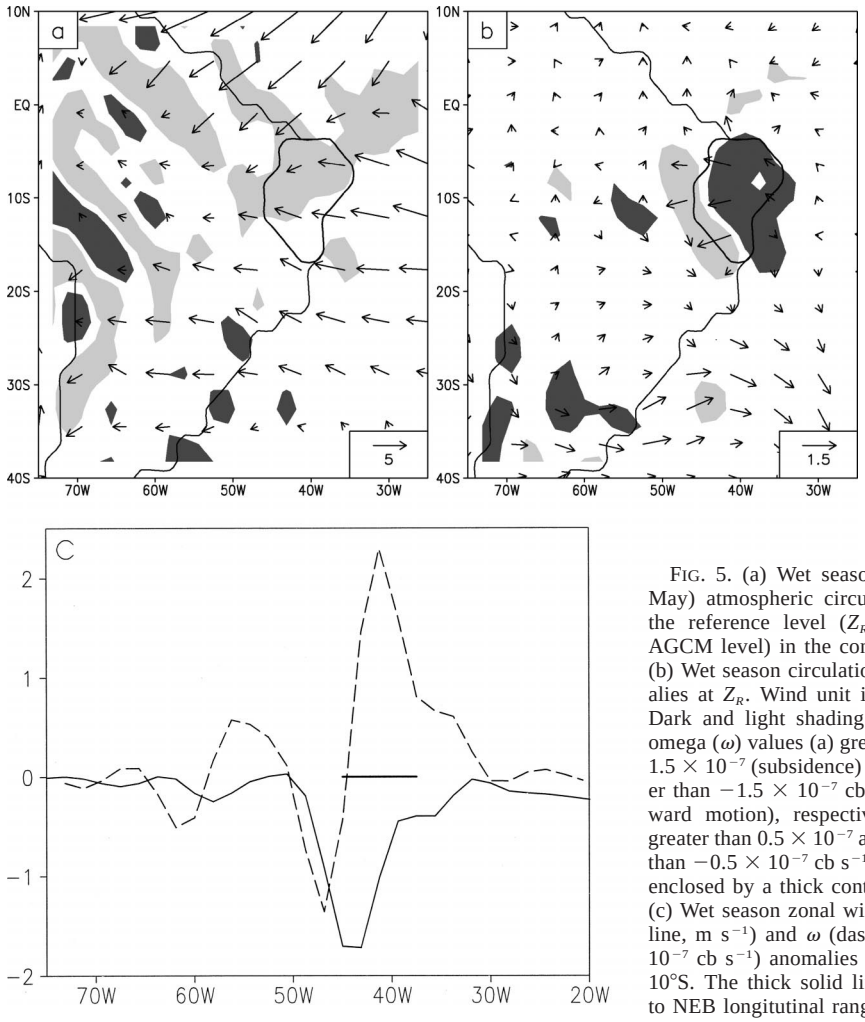

FIG. 5. (a) Wet season (Mar–May) atmospheric circulation at the reference level (Z_R, lowest AGCM level) in the control run. (b) Wet season circulation anomalies at Z_R. Wind unit is m s^{-1}. Dark and light shading refer to omega (ω) values (a) greater than 1.5×10^{-7} (subsidence) and lower than -1.5×10^{-7} cb s^{-1} (upward motion), respectively; (b) greater than 0.5×10^{-7} and lower than -0.5×10^{-7} cb s^{-1}. NEB is enclosed by a thick contour line. (c) Wet season zonal wind (solid line, m s^{-1}) and ω (dashed line, 10^{-7} cb s^{-1}) anomalies at Z_R for 10°S. The thick solid line refers to NEB longitutinal range.

decreasing moisture convergence. Third, a key problem consists of how surface net radiation reduction (e.g., due to albedo increase) is divided between sensible and latent heat flux. Increase in soil–plant (due to transpiration suppression) and aerodynamic resistances allow for dividing the surface net radiation anomaly almost evenly between sensible and latent heat flux. To increase aerodynamic resistance, decrease in roughness length is an essential ingredient. Therefore, the calculated regional climate impacts in NEB result from the cooperative action of evapotranspiration, albedo, and roughness mechanisms.

TABLE 5. Wet season (Mar–May) regional impacts (that is, area average over NEB) on omega vertical velocity (ω, 10^{-5} cb s^{-1}). Here, Z_R refers to the reference level.

Level	Anomaly
500 hPa	+0.5
700 hPa	+1.1
850 hPa	+2.0
Z_R	+0.0

6. Large-scale changes

On a larger scale, desertification leads to significant precipitation changes not confined to NEB. Statistical significance is hereafter evaluated by the sign test. Only the anomalies in NEB wet season (March to May) are shown and analyzed.

There is a dipole of statistically significant and pronounced precipitation anomalies between NEB and the oceanic belt close to the northernmost part of NEB (NNEB). Precipitation decreases in NEB (as previously shown in section 5) and increases in NNEB (Fig. 3b). The precipitation anomaly dipole is mainly due to

TABLE 6. Wet season (Mar–May) regional impacts (that is, area average over NEB) on atmospheric moisture convergence (C, mm day^{-1}). Here, Z_R refers to the reference level.

Layer	C
700–500 hPa	+0.4
850–700 hPa	−0.0
Z_R–850 hPa	−1.3

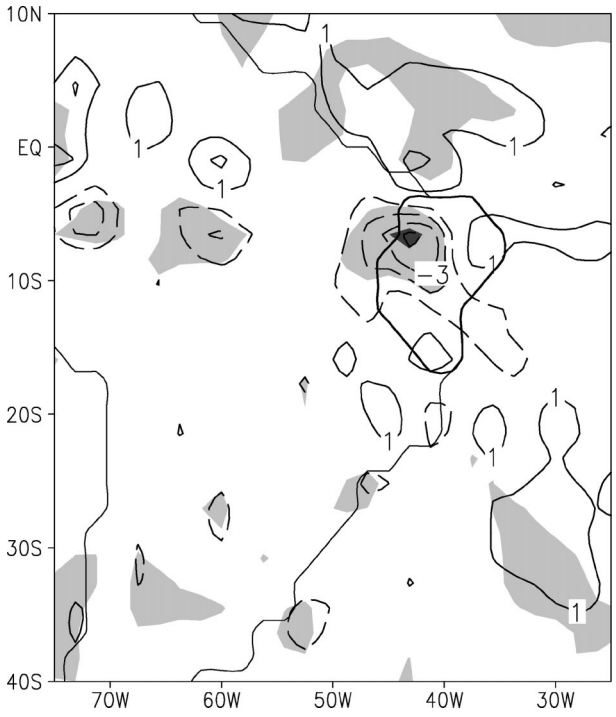

FIG. 6. Wet season (Mar–May) atmospheric moisture convergence anomalies. Contour interval is 1 mm day^{-1}. Solid (dashed) lines refer to positive (negative) values; zero line is omitted. Dark and light shading refer to high and low statistical significance anomalies, respectively, for the sign test. NEB is enclosed by a thick contour line.

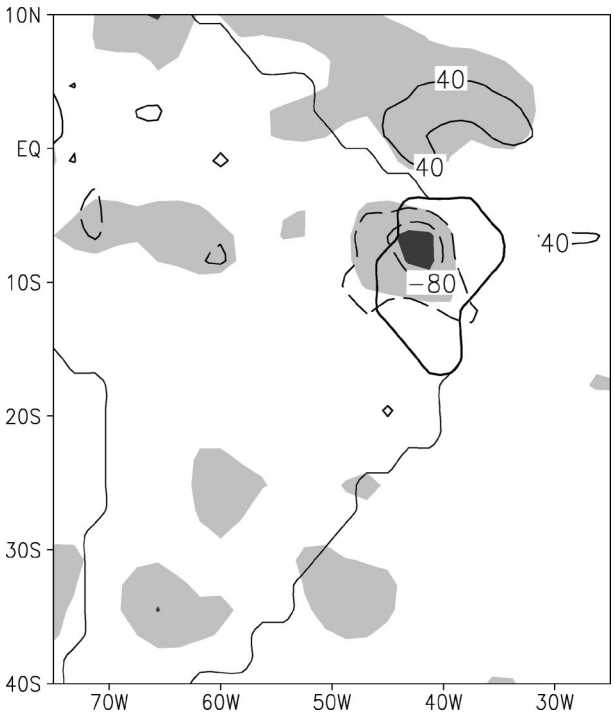

FIG. 7. Wet season (Mar–May) diabatic heating anomalies. Contour interval is 40 W m^{-2}. Lines and shading are as in Fig. 6.

changes in moisture convergence (Fig. 6). In general, where precipitation increases (NNEB), diabatic heating and upward motion anomalies are found; where it decreases (NEB), diabatic cooling and subsidence anomalies are found (Figs. 7 and 8). This strong relation between diabatic heating and vertical motion is expected for large-scale tropical motions (e.g., Holton 1992, p. 385).

In the NEB–NNEB dipole, the anomalies of vertical motion and atmospheric circulation are confined to lower atmospheric levels, that is, 850–700 hPa. Therefore, only the anomalies for these levels are hereafter shown. In 850 hPa, atmospheric convergence anomalies are found in NNEB, and divergence anomalies, in NEB (Fig. 9a). In 700 hPa, an opposite behavior is found: atmospheric divergence anomalies in NNEB and convergence anomalies in NEB (Fig. 9b). Thus, in the NEB–NNEB dipole, the level of maximum vertical velocity anomaly magnitude is located between 850 and 700 hPa.

In 850 mb, there is an anomaly high located at the NEB western boundary (Fig. 10a). On this high, circulation anomalies are predominantly divergent; wind anomalies cross the height anomaly isolines. In the NEB region where the greatest divergence anomalies are found, small positive vorticity anomalies take place. From this region towards the Northern Hemisphere

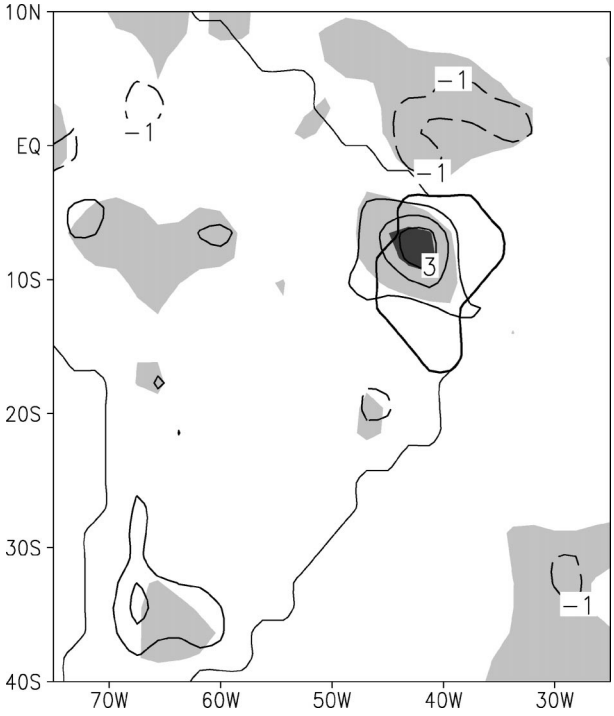

FIG. 8. Average wet season (Mar–May) omega anomalies between 850 and 200 hPa. Contour interval is 1×10^{-5} cb s^{-1}. Lines and shading are as in Fig. 6.

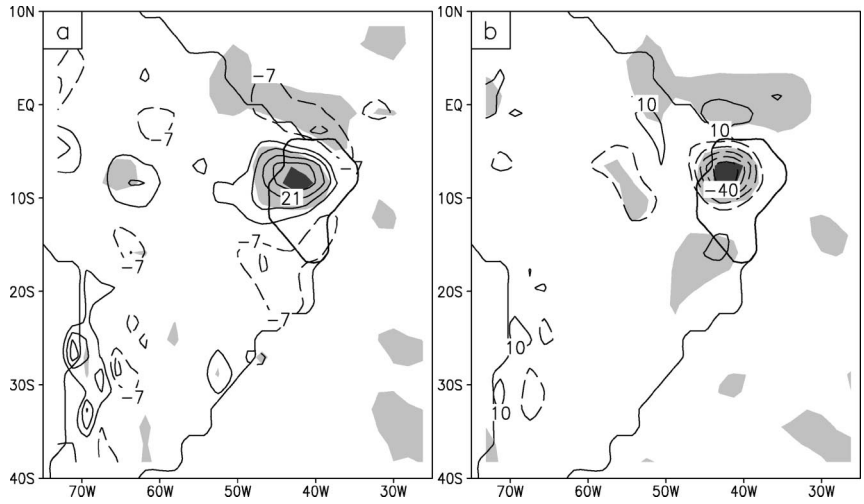

FIG. 9. Wet season (Mar–May) atmospheric divergence anomalies at (a) 850 and (b) 700 hPa. Contour interval is 7×10^{-7} in (a) and 1×10^{-6} s^{-1} in (b). Lines and shading are as in Fig. 6.

(NH), the easterly wind anomalies change direction, becoming southerly. This direction change is related to the presence of negative vorticity anomalies (cyclonic in Southern Hemisphere). Crossing the equator, the meridionally aligned wind anomalies converge into NNEB. The circulation anomalies in 10°S–5°N, 55°–40°W resemble the mixed wave pattern studied by Gill (1980), albeit more meridionally confined in NH. In 700 mb, over NEB, there is a clear cyclonic anomaly circulation associated to an anomaly low (Fig. 10b). Over NNEB, the anomaly circulation is dominated by its divergent component. A meridional southward anomaly flow leaves NNEB and arrives at NEB, resulting in divergence over NNEB.

In NEB and NNEB, the 850- and 700-hPa circulation anomalies are opposite, suggesting that the layer between 850 and 700 hPa could be responding to NEB land cover change as in isolated layer. In this shallow ~1.5-km-depth layer, the first baroclinic mode would prevail. The horizontal length scale following Gill (1980) would be of only 3°, that is, about 1/3 of the value calculated taking all troposphere depth (~10 km) into account. It means that the equatorial duct would be more confined meridionally. It explains why the mixed wave circulation anomaly pattern in 850 hPa and the precipitation anomaly dipole (NEB–NNEB) shows a more meridionally confined structure. Prescribing a horizontally uniform heat sink at 5°–15°S, 46°–36°W (approximate location of NEB) and placing it at the middle level of the shallow layer between 850 and 700 hPa, the first baroclinic mode of Gill's model is able to approximately reproduce the anomaly circulation pattern in 850 and 700 hPa (not shown). In 850 mb, this mixed wave pattern leads to weak atmospheric convergence

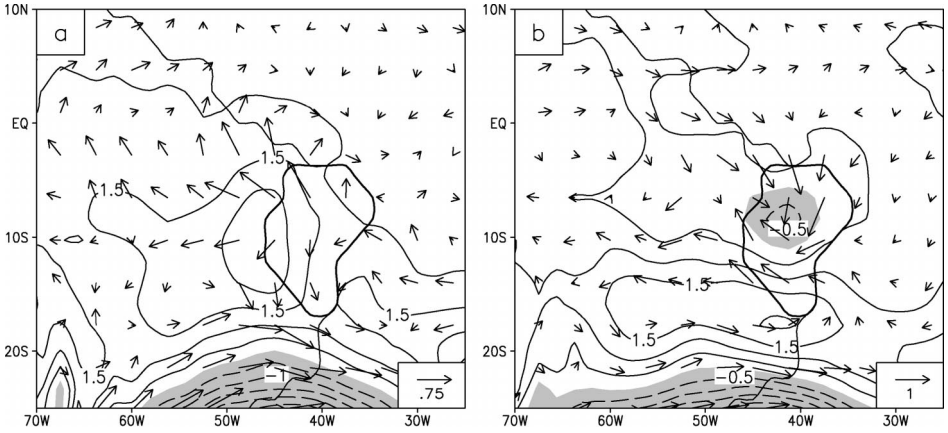

FIG. 10. Wet season (Mar–May) wind and geopotential height anomalies at (a) 850 and (b) 700 hPa. Wind unit is m s^{-1}. Contour interval is 0.5 m. Solid (dashed) lines refer to positive (negative) values; zero line is omitted. Negative values are shaded. NEB is enclosed by a thick contour line.

into NNEB. We conjecture that, by positive feedback mechanisms, this weak convergence may increase and give rise to the positive precipitation anomaly found at NNEB.

7. Summary and conclusions

The climatic impacts of a large-scale desertification in northeast Brazil (NEB) are assessed by using the CPTEC–COLA AGCM at T62L28 resolution. Two numerical runs are performed. In the control run, NEB is covered by its natural vegetation (most of NEB is covered by *caatinga*); in the desertification run, NEB vegetation is changed to desert (bare soil). Each run consists of five 1-yr numerical integrations. The results for the NEB wet season (March–May) are shown and analyzed.

Desertification results in hydrological cycle weakening: precipitation, evapotranspiration, atmospheric moisture convergence, and runoff decrease. Surface net radiation decreases and this reduction is almost evenly divided between sensible and latent heat flux. At the reference level (lowest AGCM level, about 970 hPa for NEB), easterly flow is enhanced due to decrease in roughness length. Precipitation and evapotranspiration decrease. Diabatic heating decreases (mainly due to latent heat release reduction) and, to keep atmospheric energy balance, adiabatic warming increases. This is related to subsidence anomalies mainly confined at lower atmospheric levels, reaching maximum magnitude between 850 and 700 hPa. Therefore, atmospheric divergence anomalies are found below 850 hPa, and convergence anomalies above 700 hPa. The low-level atmospheric divergence anomalies are responsible for the vertically integrated moisture convergence reduction. The calculated regional climate impacts result from the cooperative action of plant transpiration suppression, albedo increase, and roughness length decrease.

On a larger scale, desertification leads to significant precipitation changes not confined to NEB. Precipitation increase in the oceanic belt close to the northernmost part of NEB (NNEB). In this NEB–NNEB dipole, the anomalies of vertical motion and atmospheric circulation are confined to lower atmospheric levels, that is, 850–700 hPa. At these levels, circulation anomalies resemble the linear baroclinic response of a shallow atmospheric layer (850–700 hPa) to a tropical heat sink placed over NEB at the middle-layer level. In NEB, atmospheric divergence anomalies are found in 850 hPa, while convergence anomalies are found in 700 hPa. The more meridionally confined structure of the precipitation anomaly dipole (NEB–NNEB) is related to the relatively shallow diabatic heating vertical profile that has a maximum between 850 and 700 hPa. The heat sink at NEB generates a mixed wave structure at 850 hPa, and this leads to a weak convergence over the NNEB. We conjecture that, by positive feedback mechanisms, this weak convergence may increase and give rise to the positive precipitation anomaly found at NNEB.

Therefore, NEB climate does show sensitivity to an extreme vegetation change to desert (bare soil). This conclusion ratifies and expands previous assessments based on 45-day integrations using simple land surface parameterizations within a low-resolution AGCM (Sud and Fennessy 1982, 1984) and complements the study of Dirmeyer and Shukla (1996), which did not find significant precipitation changes due to replacement of NEB land cover by semidesert vegetation. In the wet season, when the changes have the greatest magnitude, our results show precipitation decrease of about 0.9 mm day^{-1}. Precipitation changes are not confined to NEB, but extend to NNEB. The present work shows the possibility of significant and pronounced climate impacts, on both regional and large scales, if the environmental degradation of NEB biomes continues unchecked.

Desertification is a complex phenomenon that involves other important processes that are not in general represented in AGCMs (and are also not represented in the AGCM used in the present work); for instance, the effect of desert dust on cloud properties and precipitation. In desert regions, there is high production of dust particles (e.g., by wind erosion on bare soil surface), and the smaller particles can be vertically and horizontally transported over large distances (Skidmore 1986). For the Sahara, Rosenfeld et al. (2001) suggests that the effect of dust on cloud properties is to inhibit precipitation. Precipitation decrease from clouds affected by desert dust could result in drier soil, which in turn could raise more dust, thus favoring further precipitation decrease. The lack of this process, as well as others such as soil salinization, soil erosion by overland runoff, etc., should be regarded as limitations of the AGCM used. The conclusions of the present work should be appreciated taking this limitation into account.

Acknowledgments. The present work is part of the first author's doctoral thesis under the guidance of the second author, and was partially supported by a grant from the National Council for Scientific and Technological Development of Brazil (CNPq). The authors would like to thank Drs. B. J. Turcq, M. H. Costa, H. R. Rocha, S. H. Franchito, J. A. Marengo, and L. A. Candido for useful comments and suggestions. Computational assistance from Dr. E. J. P. Rocha is gratefully acknowledged.

REFERENCES

Cavalcanti, I. F. A., and Coauthors, 2002: Global climatological features in a simulation using the CPTEC–COLA AGCM. *J. Climate,* **15,** 2965–2988.

Charney, J. G., 1975: Dynamics of deserts and drought in the Sahel. *Quart. J. Roy. Meteor. Soc.,* **101,** 193–202.

——, W. J. Quirk, S. H. Chow, and J. Kornfield, 1977: A comparative study of the effects of albedo change on drought in semi-arid regions. *J. Atmos. Sci.,* **34,** 1366–1385.

CONAMA, cited 1997: Resolução nº 238, de 22 de dezembro de 1997—Política Nacional de Controle da Desertificação (in Por-

tuguese). [Available online at http://www.mma.gov.br/port/conama/res/res97/res23897.html.]

Dickinson, R. E., 1992: Changes in land use. *Climate System Modeling,* K. E. Trenberth, Ed., Cambridge University Press, 689–701.

Dirmeyer, P. A., and J. Shukla, 1996: The effect on regional and global climate of expansion of the world's deserts. *Quart. J. Roy. Meteor. Soc.,* **122,** 451–482.

Dorman, J. L., and P. J. Sellers, 1989: A global climatology of albedo, roughness length and stomatal resistance for atmospheric general circulation models as represented by the Simple Biosphere model (SiB). *J. Appl. Meteor.,* **28,** 833–855.

Ferreira, D. G., H. P. Melo, F. R. Rodrigues Neto, P. J. S. Nascimento, and V. Rodrigues, 1994: Avaliação do quadro de desertificação no Nordeste do Brasil: Diagnósticos e perspectivas (in Portuguese). *Proc. National Conf. on Desertification,* Fortaleza, Brazil, Fundação Grupo Esquel Brasil, 7–55. [Available from Fundação Grupo Esquel Brasil, SAS Quadra 06 Block ''K'' - Ed. Belvedere - Sala 801-A, 70070-915, Brasília, DF, Brazil.]

Gill, A. E., 1980: Some simple solutions for heat-induced tropical circulation. *Quart. J. Roy. Meteor. Soc.,* **106,** 447–462.

Hastenrath, S., and L. Heller, 1977: Dynamics of climatic hazards in northeast Brazil. *Quart. J. Roy. Meteor. Soc.,* **103,** 77–92.

Holton, J. R., 1992: *An Introduction to Dynamic Meteorology.* Academic Press, 511 pp.

Kinter, J. L., III, and Coauthors, 1997: The COLA atmosphere–biosphere general circulation model. Vol. 1: Formulation. COLA Tech. Rep. 51, Calverton, MD, 46 pp.

Lau, K. M., J. H. Kim, and Y. Sud, 1996: Intercomparison of hydrologic processes in AMIP GCMs. *Bull. Amer. Meteor. Soc.,* **77,** 2209–2227.

Marengo, J. A., and Coauthors, 2003: Assessment of regional seasonal rainfall predictability using the CPTEC/COLA atmospheric GCM. *Climate Dyn.,* **21,** 459–475.

McGuffie, K., and A. Henderson-Sellers, 2001: Forty years of numerical climate modelling. *Int. J. Climatol.,* **21,** 1067–1109.

MMA, 2000: Desertification. Ministry of the Environment National Rep., Brasília, Brazil, 20 pp. [Available from Ministério do Meio Ambiente, Secretaria de Recursos Hídricos, SGAN Q 601 Lote 01 - Ed. Sede CODEVASF - 40 andar - Sala 417, 70830-901, Brasília, DF, Brazil.]

Nobre, C. A., and L. C. B. Molion, 1988: The effects of climatic variations on agriculture in Northeast Brazil: the climatology of droughts and drought prediction. *The Impact of Climatic Variations on Agriculture: Assessments in Semi-Arid Regions,* M. L. Parry, T. R. Carter, and N. T. Konijin, Eds., Kluwer Academic, 305–323.

——, P. J. Sellers, and J. Shukla, 1991: Amazonian deforestation and regional climate change. *J. Climate,* **4,** 957–988.

Oyama, M. D., and C. A. Nobre, 2003: A new climate-vegetation equilibrium state for Tropical South America. *Geophys. Res. Lett.,* **30,** 2199, doi:10.1029/2003GL018600.

——, E. J. P. Rocha, and C. A. Nobre, 2000: Estudo preliminar sobre o tempo de ''spin-up'' da umidade do solo no Modelo Climático do CPTEC (in Portuguese). *Proc. 11th Brazilian Congress of Meteorology,* Rio de Janeiro, Brazil, Sociedade Brasileira de Meteorologia, 1085–1094. [Available from Instituto Nacional de Pesquisas Espaciais, Centro de Previsão de Tempo e Estudos Climáticos, Rod. Presidente Dutra, km 40, 12630-000, Cachoeira Paulista, SP, Brazil.]

Rosenfeld, D., Y. Rudich, and R. Lahav, 2001: Desert dust suppressing precipitation: A possible desertification feedback loop. *PNAS,* **98,** 5975–5980.

Sá, I. B., G. A. Fotius, and G. R. Riché, 1994: Degradação ambiental e reabilitação natural no trópico semi-árido brasileiro (in Portuguese). *Proc. National Conf. on Desertification,* Fortaleza, Brazil, Fundação Grupo Esquel Brasil, 310–331. [Available from Fundação Grupo Esquel Brasil, SAS Quadra 06 Bloco ''K'' - Ed. Belvedere - Sala 801-A, 70070-915, Brasília, DF, Brazil.]

Sato, N., P. J. Sellers, D. A. Randall, E. K. Schneider, J. Shukla, J. L. Kinter III, Y. Y. Hou, and E. Albertazzi, 1989: Implementing the Simple Biosphere model (SiB) in a General Circulation Model: Methodology and results. NASA Contractor Rep. 185509, 76 pp.

Sellers, P. J., 1992: Changes in land use. *Climate System Modeling,* K. E. Trenberth, Ed., Cambridge University Press, 451–490.

Shukla, J., and Y. Mintz, 1982: Influence of land-surface evaporation on Earth's climate. *Science,* **215,** 1498–1501.

Silva, V. P. R., A. A. Correia, and M. S. Coelho, 1998: Time trend analysis of the rainfall series in the Northeast Brazil (in Portuguese). *Rev. Bras. Eng. Agríc. Ambiental,* **2,** 111–114.

Skidmore, E. L., 1986: Soil erosion by wind: An overview. *Physics of Desertification,* F. El-Baz and M. H. A. Hassan, Eds., Martinus Nijhoff, 261–273.

Stull, R. B., 1988: *An Introduction to Boundary Layer Meteorology.* Kluwer Academic, 666 pp.

Sud, Y. C., and M. Fennessy, 1982: A study of the influence of surface albedo on July circulation in semi-arid regions using the GLAS GCM. *J. Climatol.,* **2,** 105–125.

——, and ——, 1984: Influence of evaporation in semi-arid regions on the July circulation: A numerical study. *J. Climatol.,* **4,** 383–398.

——, J. Shukla, and Y. Mintz, 1988: Influence of land surface roughness on atmospheric circulation and precipitation: A sensitivity study with a general circulation model. *J. Appl. Meteor.,* **27,** 1036–1054.

——, W. C. Chao, and G. K. Walker, 1993: Dependence of rainfall on vegetation: Theoretical considerations, simulation experiments, observations and inferences from simulated atmospheric sounding. *J. Arid Environ.,* **25,** 5–18.

——, G. K. Walker, J.-H. Kim, G. E. Liston, P. J. Sellers, and W. K.-M. Lau, 1996: Biogeophysical consequences of a tropical deforestation scenario: A GCM simulation study. *J. Climate,* **9,** 3225–3247.

Xue, Y., and J. Shukla, 1993: The influence of land surface properties on Sahel climate. Part 1: Desertification. *J. Climate,* **6,** 2232–2245.

——, P. J. Sellers, J. L. Kinter, and J. Shukla, 1991: A simplified biosphere model for global climate studies. *J. Climate,* **4,** 345–364.

Zeng, N., R. E. Dickinson, and X. Zeng, 1996: Climatic impact of Amazon deforestation—A mechanistic model study. *J. Climate,* **9,** 859–883.